arXiv:1403.5742v1 [cond-mat.str-el] 23 Mar 2014

Magnon dispersion and hole motion in 2D frustrated antiferromagnets with 4-sublattice structures

Satyaki Kar
Saha Institute of Nuclear Physics, Salt Lake, Kolkata 700064, India.

We study a two dimensional spin-$\frac{1}{2}$ $J_1 - J_2$ antiferromagnet in a square lattice using the linearized spin wave theory respecting the 4-sublattice nature of the underlying magnetic lattice (see figure 1). The dispersion of the optical and acoustic magnon modes are obtained about the stable Neel ordered and columnar reference states for small and large values of $\lambda(= J_2/J_1)$ respectively. The single hole spectral behavior in a 2D $t - J_1 - J_2$ model, for small frustration, is then calculated within the non-crossing approximation. Our results match fairly well with exact diagonalization results from a 4×4 cluster and are found to be an improvement over the earlier results obtained using similar Self consistent Born approximation. Hole spectral features and their evolution with λ resulting in "water-fall"-like smooth spectral weight transfer is discussed. Hole energy bands are identified and the corresponding energy-shift and reduction in width with spin-frustration are indicated. Our magnon dispersion results and hole spectral calculations can be utilized to understand the Neutron diffraction and ARPES results from 2D or quasi-2D frustrated spin systems.

I. INTRODUCTION

Geometrically frustrated quantum Heisenberg antiferromagnet (AF) in low dimensions have long emerged as a popular field of study in condensed matter in understanding the magnetic properties of various magnetic materials with layered structures. As for example, the key to charge transport in the newly discovered Iron-based high temperature superconductors[1, 2] is believed to exist in their spin-frustrated conducting FeAs layers. A

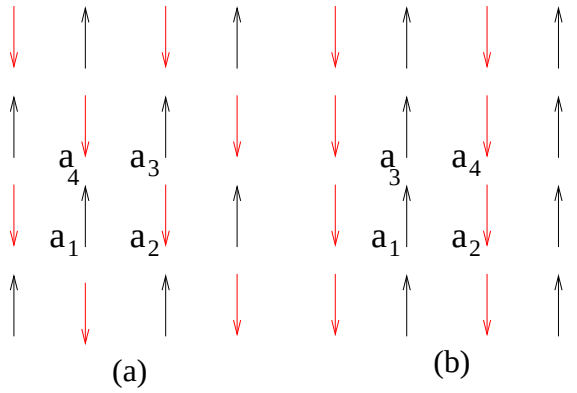

FIG. 1: The (a) Neel ordered $k = (\pi, \pi)$ reference state and (b) columnar $(\pi, 0)$ reference state with 4 sublattices. Here a_i denotes the i-th sublattice.

two dimensional (2D) $J_1 - J_2$ model, frustrated due to the competing J_1 and J_2 AF interactions, gives different phases in different parameter range of $\lambda = J_2/J_1$. A classically Neel-ordered phase with (π, π) magnetic long range order is formed for small λ whereas a columnar $(\pi, 0)$ or $(0, \pi)$ ordered phase is obtained at large values of λ. Quantum fluctuations, on the other hand, result in a disordered spin liquid phase in such system for intermediate values of frustration: $0.4 < \lambda < 0.6$[3–5]. While studying this model, Chandra et al.[6] used conventional spin wave theory to predict a spin-liquid ground state for large values of frustration. Dagotto et al.[7] used exact diagonalization and showed how magnetization changes with λ indicating Neel ordered AF phase and columnar phase at small and large values of λ respectively. Rather recently, Li et al.[5] used a bosonic resonating valence-bond ansatz to show that stable spin liquid phases are present in such systems for $0.4 < \lambda < 0.6$.

The present work involves studying the spin ordered phases of a spin-$\frac{1}{2}$ 2D $J_1 - J_2$ model. We use linear spin wave (LSW) approximation to identify the spin-wave modes about the (π, π) and $(\pi, 0)$ reference states for $\lambda < 0.4$ and $\lambda > 0.6$ respectively and considered spin wave expansion about these states. We have also studied $t - J_1 - J_2$ model in an undoped frustrated antiferromagnet to witness the hole motion in it. Self consistent Born approximation (SCBA) is used for that purpose to obtain the single hole spectra. We mention here that similar calculations were also done in ref.[8] in obtaining the hole spectral functions. But our approach has a fundamental difference from theirs which we will address, along with the comparative results, in section 4. The main objective of this paper is to form a building block in studying magnon and hole spectral behavior in a 2D frustrated antiferromagnet that can be realized and compared with Neutron diffraction or angle-resolved photo-emission spectroscopy (ARPES) results obtained from various frustrated quasi-2D spin systems like $Li_2VO(Si, Ge)O_4$[9] or the FeAs superconducting compounds[10, 11].

The paper is organized as follows: Section 2 is the formulation part which describes a 2D $J_1 - J_2$ spin Hamiltonian and the conventional linear spin wave analysis on it. In Section 3, we discuss the Bogoliubov transformation yielding the magnon modes for different values of λ. Section 4 deals with the hole hopping using a $t - J_1 - J_2$ model. SCBA is used to obtain the hole spectral functions and the spectral behavior are discussed in detail. Finally in section 5, we summarize our results and dis-

cuss the immediate future plans that we have related to this work.

II. FORMULATION

In a 2D square lattice that we consider, a $J_1 - J_2$ Heisenberg spin Hamiltonian is given as

$$H_{J1J2} = H_{J1} + H_{J2} = J_1 \sum_{<i,j>} \mathbf{S_i}.\mathbf{S_j} + J_2 \sum_{<<i,j>>} \mathbf{S_i}.\mathbf{S_j} \quad (1)$$

where $< i, j >$ of H_{J1} and $<< i, j >>$ of H_{J2} represent indices for the nearest neighbor (NN) and next nearest neighbor (NNN) site-pairs respectively and S denotes the spin. H_{J1} produces two opposite spin sublattices and at low temperature, the elementary excitations of spin waves or magnons are created on top of this (π, π) AF reference state.

H_{J2} , however, involves NNN AF spin interactions that do not communicate between $\uparrow$ and $\downarrow$ sublattice caused by H_{J_1}. Rather within each such sublattice, it creates two sublattices on its own. Thus an overall outer product of four spin sublattices are formed in a $J_1 - J_2$ antiferromagnet[12] (see Fig.1).

This $J_1 - J_2$ model represents a frustrated spin system as the J_1 and J_2 terms prefer different spin-orders to be the ground state of the system. For comparatively small strength of J_2 with the factor $\lambda = J_2/J_1$ being a small fraction, the (π, π) spin order describes the reference state of the system and the spin excitations appear above this vacuum state. At large enough value of λ however, a $(\pi, 0)$ or $(0, \pi)$ ordered state becomes the zero spin deviation vacuum state of the system.

Here we use LSW approximation[13] to find the magnon modes of the $J_1 - J_2$ model about (π, π) and $(\pi, 0)$ spin ordered states at small and large values of λ respectively.

Figure 1 illustrates the real space snapshot of the (π, π) and $(\pi, 0)$ reference states with the indication of the 4 sublattices. The unit vectors in real space for the $J_1 - J_2$ model are $a_1 = 2\hat{x}$ and $a_2 = 2\hat{y}$ (and $b_1 = \pi\hat{y}$ and $b_2 = \pi\hat{x}$ in the Fourier space). The 1st Brillouin zone (BZ) is a square with corners at $(\pm\pi/2, \pm\pi/2)$. The lattice is broken down to 4 sublattices and the LSW calculation gives two different spin wave modes each with degeneracy 2 (for the spin up-down symmetry).

The bosonic spin wave operators $a_{i,\mathbf{r}}$'s are defined as $S_{z,i} = S - a^\dagger_{i,\mathbf{r}} a_{i,\mathbf{r}}$ $(-S + a^\dagger_{i,\mathbf{r}} a_{i,\mathbf{r}})$ for $\uparrow$ $(\downarrow)$ sublattices and they follow the Fourier transformation: $a_{i,\mathbf{k}} = \sqrt{\frac{4}{N}} \sum_{\mathbf{r}\epsilon i} a_{i,\mathbf{r}}\ e^{i\mathbf{k}.\mathbf{r}}$, $\mathbf{k}$ being the Bloch wave vectors within the BZ. This transforms our Eq.1 to: $H = E_0 + \sum_k < a_k|A|a_k >$ with E_0 being a constant term and $|a_k >= (a_{1,\mathbf{k}}, a^\dagger_{2,-\mathbf{k}}, a_{3,\mathbf{k}}, a^\dagger_{4,-\mathbf{k}})$. For small λ with

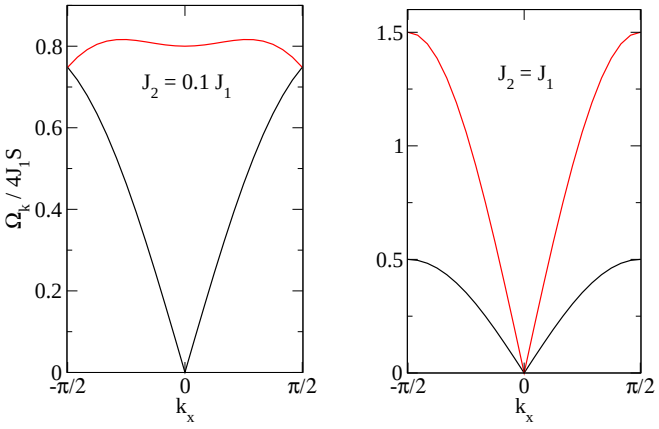

FIG. 2: Left:Acoustic (black) and optical (red or grey) magnon modes about (π, π) reference state. Right: Acoustic magnon modes about $(\pi, 0)$ reference state. Both the plots have $k_y = 0$.

(π, π) reference state, we find

$$A = 4J_1S \begin{pmatrix} 1-\lambda & \frac{cos\ k_x}{2} & \lambda\Gamma_k & \frac{cos\ k_y}{2} \\ \frac{cos\ k_x}{2} & 1-\lambda & \frac{cos\ k_y}{2} & \lambda\Gamma_k \\ \lambda\Gamma_k & \frac{cos\ k_y}{2} & 1-\lambda & \frac{cos\ k_x}{2} \\ \frac{cos\ k_y}{2} & \lambda\Gamma_k & \frac{cos\ k_x}{2} & 1-\lambda \end{pmatrix}$$

with $\Gamma_k = \frac{1}{2}(\cos(k_x + k_y) + \cos(k_x - k_y))$ and for large λ with $(\pi, 0)$ reference state, we obtain

$$A = 4J_1S \begin{pmatrix} \lambda & \frac{cos\ k_x}{2} & \frac{cos\ k_y}{2} & \lambda\Gamma_k \\ \frac{cos\ k_x}{2} & \lambda & \lambda\Gamma_k & \frac{cos\ k_y}{2} \\ \frac{cos\ k_y}{2} & \lambda\Gamma_k & \lambda & \frac{cos\ k_x}{2} \\ \lambda\Gamma_k & \frac{cos\ k_y}{2} & \frac{cos\ k_x}{2} & \lambda \end{pmatrix}.$$

III. MAGNON DISPERSION

This Hamiltonian is diagonalized using Bogoliubov transformation which is a canonical transformation where new bosonic operators α_k's are introduced as

$$a_{i,\mathbf{k}} = U_{i,jo}(\mathbf{k})\alpha_{jo,\mathbf{k}} + U_{i,je}(\mathbf{k})\alpha^\dagger_{je,-\mathbf{k}}, \quad (i\ \ odd)$$
$$a^\dagger_{i,-\mathbf{k}} = U_{i,jo}(\mathbf{k})\alpha_{jo,\mathbf{k}} + U_{i,je}(\mathbf{k})\alpha^\dagger_{je,-\mathbf{k}}, \quad (i\ \ even) \quad (2)$$

where sum over jo (1, 3) and je (2, 4) are implied, U being the 4×4 coefficient matrix. The bosonization condition for the variables α requires

$$\sum_j (-1)^{i+j} U_{i,j}(\mathbf{k}) U_{i',j}(\mathbf{k}) = \delta_{i,i'} \quad (3)$$

while the diagonalization of the Hamiltonian matrix requires

$$\sum_j (A_{i,j}(\mathbf{k}) - \epsilon_l(\mathbf{k})(-1)^{l+j})\ U_{j,l}(\mathbf{k}) = 0. \quad (4)$$

$\epsilon_l(\mathbf{k})$ denoting the l-th eigen-energy mode. Non-trivial solution of Eq.4 gives the eigenvalues. Fig.2 shows the magnon modes for $k_y = 0$ for both small and large λ's.

For $\lambda < 0.5$ with (π,π) reference state, we obtain the acoustic and optical spin wave modes (as also mentioned in ref.[14]) given by $\Omega_{ac}(k) = 4J_1S\sqrt{(1-\lambda(1-\Gamma_k))^2-\gamma_k^2}$ and $\Omega_{op}(k) = 4J_1S\sqrt{(1-\lambda(1+\Gamma_k))^2-\gamma_k^2+\Gamma_k}$.

For $\lambda > 0.5$, similar calculation with $(\pi,0)$ order representing the zero-spin deviation state gives multiple acoustic modes with expressions $\Omega_1(k) = 4J_1S\sqrt{(\lambda+\frac{1}{2}cosk_y)^2-(\lambda\Gamma_k+\frac{1}{2}cosk_x)^2}$ and $\Omega_2(k) = 4J_1S\sqrt{(\lambda-\frac{1}{2}cosk_y)^2-(\lambda\Gamma_k-\frac{1}{2}cosk_x)^2}$.

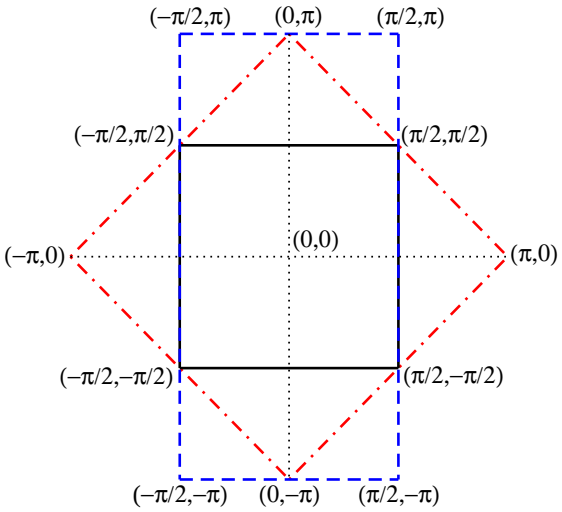

FIG. 3: (Color online) 1st Brillouin zone for $J_1 - J_2$ model (black), the J_1 antiferomagnet (red, dash-dotted) and J_2 antiferromagnet with $(\pi,0)$ reference state (blue, dashed).

Let's take a look at the Brillouin zones shown in Fig.3. Here, the BZ for our 4-sublattice magnetic picture (let's call it BZ0), a square with corners at $(\pm\pi/2, \pm\pi/2)$, is shown (black lines) along with the the Brillouin zones for the extreme cases of $J_2 = 0$ and $J_1 = 0$ respectively. For $J_2 = 0$, we have the BZ for the Neel AF, as shown by the square with dash-dotted lines in Fig.3. By band-folding the $(\pi,0)$ vector falls on the Γ point $(0,0)$. And the energy of the acoustic mode at $k = (\pi,0)$ being non-zero, we get an additional optical mode with a non-zero spin gap at the zone center of BZ0. But for $J_1 = 0$, we have, the spin fluctuations being switched off, a ground state degeneracy between $(\pi,0)$ and $(0,\pi)$ states. For the $(\pi,0)$ spin reference state that we consider here, the BZ is shown by the rectangle with dashed lines in Fig.3. In this case, the $(0,\pi)$ vectors folds back to the Γ point. And the acoustic mode energy at $k = (0,\pi)$ being zero, we no more get an optical mode and rather two distinct acoustic modes are obtained in the reduced picture. Both the modes give zero dispersion energies for $(0,\pi)$ and $(\pi,0)$ vectors and they become degenerate in the limit $\lambda \to \infty$. Our findings, for large λ are similar to the magnon dispersion results obtained using a two-sublattice picture[15].

IV. HOLE DYNAMICS

In order to incorporate hole motion in such a system we include NN hole-hopping. The resulting $t - J_1 - J_2$ Hamiltonian is thus given by

$$H_{tJ1J2} = H_{J1J2} - t\sum_{<i,j>,\sigma}(C^\dagger_{i,\sigma}C_{j,\sigma} + h.c.). \qquad (5)$$

C denoting the fermionic annihilation operators, maintaining the constraint of no double occupancy. The t term can be linearized after rewriting it in terms of spin wave operators and the slave fermions as worked out in ref.[16] for a 2D $t-J$ model. The only difference in our case will be due to having 4 sublattices and a Green's function matrix that has non-zero off-diagonal entries.

Let us consider (π,π) reference state for small λ. In this case we have coupled Dyson's equations for a 4×4 Green's function matrix:

$$G^{(n)}_{ij} = G^{(0)}_{ij} + \sum_k G^{(0)}_{ii}\Sigma^{(n)}_{ik}G^{(n)}_{kj}$$

$$i.e., \quad \sum_{k=1}^{4}(\delta_{ik} - G^{(0)}_{ii}\Sigma^{(n)}_{ik})G^{(n)}_{kj} = G^{(0)}_{ij} \qquad (6)$$

where the superscripts indicate the iteration numbers. By symmetry, all G_{ii}'s are same and off-diagonal G_{ij}'s are non-zero only if (i,j) pairs are (1,3) or (2,4). Solving matrix equation gives

$$G_{11} = \frac{G^{(0)}_{11}(1-G^{(0)}_{11}\Sigma_{11})}{(1-G^{(0)}_{11}\Sigma_{11})^2-(G^{(0)}_{11}\Sigma_{13})^2}$$
$$G_{13} = \frac{(G^{(0)}_{11})^2\Sigma_{13}}{(1-G^{(0)}_{11}\Sigma_{11})^2-(G^{(0)}_{11}\Sigma_{13})^2} \qquad (7)$$

Here argument of (k,ω) are implied for all the variables.

Within the non-crossing approximation (NCA), hole self energy expressions are obtained as

$$\begin{aligned}\Sigma_{11}(k,\omega) =& c_0[g^2_{12j}(k,q)G(k-q,\omega-\Omega_{j,q}) \\ &+ f^2_{14j}(k,q)G(k-q,\omega-\Omega_{j,q})], \\ \Sigma_{13}(k,\omega) =& c_0[g_{12j}(k,q)f_{32j}(k,q)G(k-q,\omega-\Omega_{j,q}) \\ &+ f_{14j}(k,q)g_{34j}(k,q)G(k-q,\omega-\Omega_{j,q})]\end{aligned} \qquad (8)$$

where sum over $\mathbf{q}$, j (1 and 3) and j' (2 and 4) are implied. $c_0 = \frac{16}{N}t^2$, $g_{ijl}(\mathbf{k},\mathbf{q}) = (U_{jl}(\mathbf{q})cos(k_x) + U_{il}(\mathbf{q})cos(k_x - q_x))$ and $f_{ijl}(\mathbf{k},\mathbf{q}) = (U_{jl}(\mathbf{q})cos(k_y) + U_{il}(\mathbf{q})cos(k_y - q_y))$. $\Omega_{j,q}$ denotes the j-th magnon mode energy at wave vector q and G is the eigenvalue of the Green's function matrix.

With this self-energy expression we solve the Dyson's equation (Eq.6) iteratively following SCBA to obtain

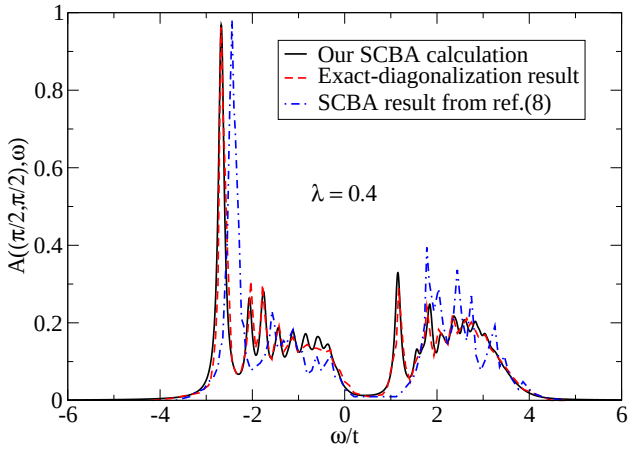

FIG. 4: $(\pi/2, \pi/2)$ spectra of a 4×4 lattice for $J_1 = 0.4t$.

the single hole spectra which is given as $A(k,\omega) = -Img[G(k,\omega)]/\pi$. The bare Green's function entries are given by $G^{(0)}_{ij}(k,\omega) = \delta_{ij}/(\omega + i\eta)$ where η is a small number (for example, in our spectral plots of Fig.5 we used $\eta = 0.02t$).

Our findings show that the general feature of the hole spectra is to have a low energy quasi-particle like excitation followed by a series of higher energy excitations called string states[16]. The lowest quasi-particle (QP) peak is found at $(\frac{\pi}{2}, \frac{\pi}{2})$ and as we increase λ from 0 to 0.4, the $(\frac{\pi}{2}, \frac{\pi}{2})$ peak gradually shifts to lower energy and reduces its strength.

Our spectral results in the $J_2 \to 0$ limit match with that of the $t - J$ model results of ref.[16]. The comparison at non-zero values of J_2 has also been made. Ref.[8] contains similar SCBA calculation of a 2D $t - J_1 - J_2$ model. But they consider only two sublattices in their calculation and ignored the actual 4 sublattice nature of the problem. In Fig.4 we show the $(\pi/2, \pi, 2)$ spectra of a 4×4 lattice at $\lambda = 0.4$ (with $J_1 = 0.4t$) obtained by our SCBA calculation with also plots from exact diagonalization (ED) and SCBA calculation taken from ref.[8]. Our results match much better with the exact result both in position and relative-strengths of the spectral peaks - corresponding to both the lowest energy QP and the high energy string excitations. We should mention here that this disagreement between the two SCBA calculations can't be completely attributed to the difference in sublattice picture used as we find fair match of numerical spectral plots and exact results even when we pursue the two-sublattice picture with equations and other details modified accordingly.

In Fig.5, we have shown the hole spectra for λ= 0.005, 0.1 and 0.3 respectively ($J_1 = 0.3t$) obtained from a 32×32 lattice for $k = (\pi/2, \pi/2)$ and $k = (0,0)$. The energy resolution of our numerical calculation is $\Delta\omega = 0.005t$ and the small parameter $\eta = 0.02t$. With these specifications, 32×32 lattice represent a large enough system to avoid the finite size effects in the spectral plots[16].

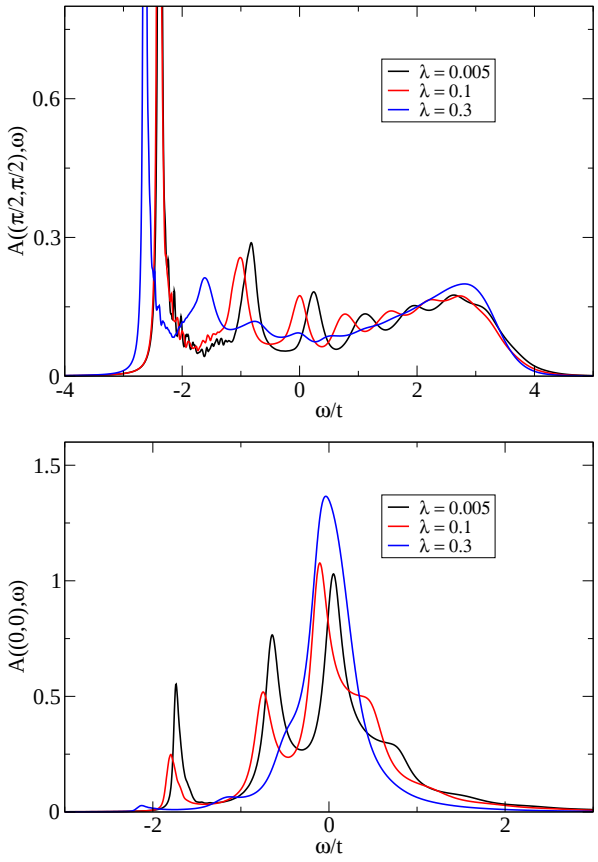

FIG. 5: (Color online) Hole spectral function $A(k,\omega)$ for $k = (\pi/2, \pi/2)$ (top) and $k = (0,0)$ (bottom) for different small values of λ at $J_1 = 0.3t$.

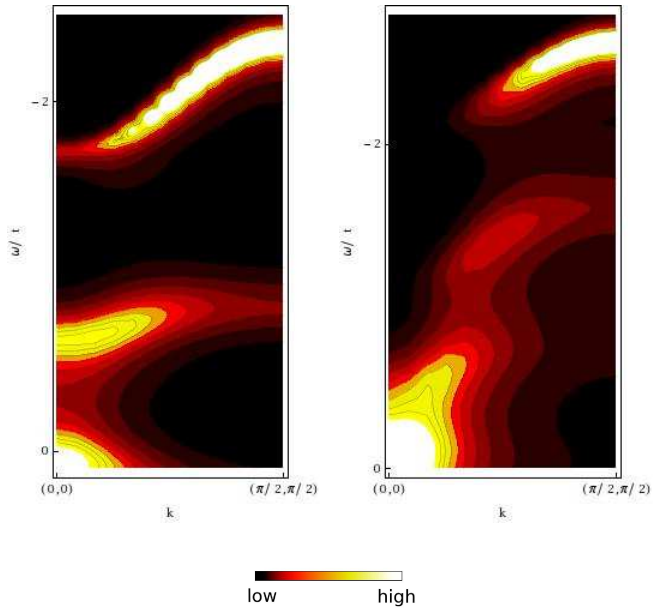

FIG. 6: (Color online) Spectral intensity along the nodal direction from $(0,0)$ to $(\pi/2, \pi/2)$ points in k space in a 48×48 lattice for $\lambda = 0.005$ (left) and $\lambda = 0.3$ (right) respectively.

A hole in a 2D $t-J$ model prefers to move with wave vector $(\pi/2,\pi/2)$. We observe that with NNN AF interaction present, this remains the case for $\lambda \leq 0.4$. In the $t-J_1-J_2$ model, with J_2 switched on starting from zero, low energy spectral peaks move to lower energies and this shift becomes more for higher values of J_2. Peaks along $(\pi/2,\pi/2)$ to $(\pi/2,0)$ directions which were already close to the lowest peak at $(\pi/2,\pi/2)$ for $\lambda=0$, becomes even closer as λ is increased. Nevertheless the $(\pi/2,\pi/2)$ peak stays the lowest energy peak as long as $\lambda \leq 0.4$. We also notice loss of intensity in the QP as well as the string states as J_2 is increased gradually. This enables a smooth transfer of spectral intensity from lowest peak at $(\pi/2,\pi,2)$ to the highest peak at $(0,0)$ resembling a water-fall as shown in Fig.6. So the effect of small frustration is the same as that of electron-phonon coupling[17] or doping[18] in smearing out the long lived well-defined QP excitations producing smooth transitions in spectral intensity from the low energy peak to the high energy peak. This so called 'waterfall'-feature in intensity is observed along the nodal direction in the ARPES results of the superconducting cuprates[19].

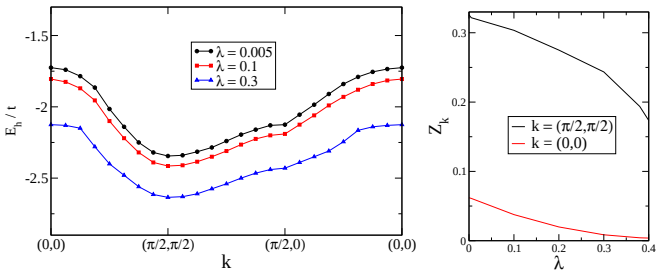

FIG. 7: (Color online) Left: Hole QP energy band along the boundary of irreducible BZ. Right: Decrease of QP residue with λ.

In Fig.7 left panel, we have constructed the QP hole energy (E_h) band along the boundary of the irreducible BZ, namely $(0,0) \rightarrow (\pi/2,\pi/2) \rightarrow (\pi/2,0) \rightarrow (0,0)$ for similar three values of λ. It clearly shows the lowest peak to be at $(\pi/2,\pi/2)$. All the QP peak positions lower in energy with an increase in J_2. At the same time the hole bandwidth W also decreases as $W \sim 2(J_1-J_2)$. This energy band construction involves defining the lowest energy excitations for different k-values as the QP excitations of the holes. With an increase in λ, the residue (Z_k) of those lowest energy peaks reduces gradually[8] as shown in Fig.7 right panel. We see that, for $\lambda \sim 0.4$, the residue for the $(0,0)$ (or (π,π)) vector almost vanishes making the QP nature for hole excitations, for such k vector, not valid anymore.

V. SUMMARY AND DISCUSSION

In this article, we have studied the spin dynamics of a 2D J_1-J_2 model and found the acoustic and optical magnon modes about the state $k=(\pi,\pi)$. Contrarily, two acoustic and no optical modes are obtained when large values of λ are considered and $k=(\pi,0)$ is used as the reference state.

Hole spectra are obtained from a 2D $t-J_1-J_2$ model for small λ. We observe the QP and string-like excitations in the spectral behavior and an energy shift and bandwidth reduction for the hole QP is also witnessed as λ is increased from zero.

With $(\pi,0)$ reference state for $\lambda > 0.6$, NN hole hopping needs to be addressed separately. Here neighbors along y prefers to align ferromagnetically while that along x prefers an AF order. We plan, in future, to extend our similar 4-sublattice calculations to obtain the hole spectral results in this highly frustrated limit and also discuss the case where the reference state implies a coexistence of both $(\pi,0)$ and $(0,\pi)$ orders[20, 21]. We also plan to extend our study to a multi-orbital $t-J_1-J_2$ model, as discussed in ref.[14, 22] in the limit of large frustration (generally $\lambda \sim 2$), so that comparison with the ARPES results obtained from FeAs superconduting materials[10, 11] becomes possible.

VI. ACKNOWLEDGEMENT

S. Kar acknowledges funding support from Saha Institute of Nuclear Physics, India.

[1] Y. Kamihara *et al.*, JACS 128,10012 (2006).
[2] Y. Kamihara *et al.*, JACS 130, 3296 (2008).
[3] H. J. Schulz *et al.*, EPL 18,355 (1992).
[4] J. Oitmaa *et al.*, Phys. Rev. B 54,3022 (1996).
[5] T. Li *et al.*, Phys. Rev. B 86,075111 (2012).
[6] P. Chandra *et al.*, Phys. Rev. B 38,9335 (1988).
[7] E. Dagotto *et al.*, Phys. Rev. Lett. 63,2148 (1989).
[8] I. J. Hamad *et al.*, Phys. Rev. B 77,014410 (2007).
[9] R. Melzi *et al.*, Phys. Rev. Lett. 85, 1318 (2000).
[10] Y. Xia *et al.*, Phys. Rev. Lett. 103, 037002 (2009).
[11] K. Nakayama *et al.*, Phys. Rev. Lett. 105, 197001 (2010).
[12] C. Xu *et al.*, Phys. Rev. B 78, 020501(R) (2008).
[13] E. Manousakis, Rev. Mod. Phys. 63,1 (1991).
[14] E. Manousakis, Phys. Rev. B 79,220509 (2009).
[15] D. X. Yao *et al.*, Phys. Rev. B 78,052507 (2008).
[16] Z. Liu *et al.*, Phys. Rev. B 45,2425 (1992).
[17] S. Kar *et al.*, Phys. Rev. B 78,064508 (2008).
[18] S. Kar *et al.*, Phys. Rev. B 84,205107 (2011).
[19] A. Damascelli *et al.*, Rev. Mod. Phys. 75,473 (2003).
[20] P. Caretta *et al.*, Phys. Rev. Lett. 88, 047601 (2002).
[21] I. J. Hamad *et al.*, Physica B 398,416 (2007).
[22] R. Yu *et al.*, Phys. Rev. B 89,024509 (2014).